Supporting Information

for

Lighting Up Healing: Green Light-Driven Dual Gasotransmitters Release Against MRSA Wound Infections

Yanyan Hou[1,2,#], Yuze Wang[1,#], Ping Yang[3,#], Zhetao Shen[4], Xueli Wang[4], Jinquan Chen[4], Youjun Yang[2,*], Daijie Chen[3,*], Xuhong Qian[1,2,*], Xiao Luo[1,*].

[1] Shanghai Engineering Research Center of Molecular Therapeutics and New Drug Development, School of Chemistry and Molecular Engineering, East China Normal University, Dongchuan Road 500, Shanghai 200241, China. [2] State Key Laboratory of Bioreactor Engineering, Shanghai Key Laboratory of Chemical Biology, School of Pharmacy, East China University of Science and Technology, Meilong Road 130, Shanghai 200237, China. [3.] School of Pharmacy, Shanghai Jiao Tong University, Shanghai 200240, China. [4.] State Key Laboratory of Precision Spectroscopy, East China Normal University, Dongchuan Road 500, Shanghai 200241, China.

Emails:
X. Luo: xluo@chem.ecnu.edu.cn.
X. Qian: xhqian@ecnu.edu.cn.
D. Chen: hccb001@163.com.
Y. Yang: youjunyang@ecust.edu.cn.

#These authors contributed equally to this work

Table of Contents

General methods

Unless otherwise specified, all chemicals were purchased from reputable commercial suppliers in China and used as received without further purification. Thin-layer chromatography (TLC) was performed on silica gel plates to monitor the reaction progress. For column chromatography, silica gel (300-400 mesh) from Qingdao Ocean Chemicals was employed.

The ^{1}H-NMR and ^{13}C-NMR spectra were recorded using Bruker AVANCE III 500 or Bruker AVANCE III 600 spectrometers, with tetramethylsilane or solvent residue as the internal standard. Chemical shifts are reported in parts per million (ppm). High-resolution mass spectrometry (HRMS) data were acquired using a maXis Impact spectrometer. UV-Vis absorption and fluorescence emission spectra were recorded using Shimadzu UV-1900i and Agilent Cary Eclipse instruments, respectively. High-performance liquid chromatography data were collected using a Shimadzu LC-16p system. Gas chromatographic data were obtained with a GC2060 gas chromatograph (Shanghai Ruimin Instrument Co., Ltd.). The detailed GC conditions were as follows: Column: 2 m × 3 mm OD stainless steel column packed with Molecular Sieve 5Å (60/80 mesh); Carrier gas: Nitrogen; Flow rate: 30 mL/min; Detector: Flame ionization detector (FID); Column temperature: 120 °C; Detector temperature: 230 °C. CO release was detected using a Dräger Pac 6500 electrochemical detector (Shanghai Jingong Industrial Co., Ltd.). Electron paramagnetic resonance spectra were recorded on an EMX-8/2.7 spectrometer (Bruker, USA). Confocal fluorescence images were obtained using an Olympus FV 3000 system, and bright-field images were captured with an OPTIKA IM-3 microscope. Scanning electron microscope (SEM) images were acquired with an S-4800 cold field emission SEM (Hitachi High-tech Co., Ltd.). Cytotoxicity data were measured using a Varioskan LUX multifunctional enzyme marker (Thermo Scientific). Mice were anesthetized using a gas anesthesia machine (Medical Supplies & Services Int. Ltd.).

Experimental Section

Photoirradiation of AhCR565 in Cuvettes

A 5 mM stock solution of **AhCR565** was prepared in DMSO, and the test solution was subsequently prepared by diluting the stock into PBS (10 mM, pH = 7.4) containing 0.5% DMSO. Photolysis experiments were conducted using a parallel photoreactor. The absorption and emission spectra of the test solution were recorded under light irradiation at wavelengths of 365 nm (50 mW/cm^2), 400 nm (46 mW/cm^2), 450 nm (48 mW/cm^2), 520 nm (30 mW/cm^2), 560 nm (12 mW/cm^2), and white light (1 W). The irradiation was terminated until the absorption and fluorescence spectra stop increasing. The maximum absorption or maximum fluorescence intensity of each acquired spectrum was plotted against the irradiation time (seconds or mins).

Photolysis experiments were conducted in a parallel photoreactor (Photosyn-10 model) from Shanghai Quanhuan Technology Co., Ltd.

Measurement of the quantum yield for the photoconversion of AhCR565 to Ah565.

The quantum yield of photolysis is defined as follows.

$$\Phi = \frac{number\ of\ reacted\ molecules\ per\ time\ unit}{number\ of\ photons\ absorbed\ per\ time\ unit}$$

The number of photons absorbed per unit time (photon flux) at each wavelength (365 nm, 400 nm, 450 nm, 520 nm and 560 nm) was determined using Reinecke's salt actinometry in an aqueous solution, in accordance with established literature protocols.[1] The underlying photochemical reaction of Reinecke's salt is illustrated below:

$$[Cr(NH_3)_2(SCN)_4]^- + H_2O \xrightarrow{h\upsilon} [Cr(NH_3)_2(SCN)_3(H_2O)] + SCN^-$$

$$Fe^{3+} + SCN^- \longrightarrow Fe(SCN)^{2+}$$

The number of absorbed photons was determined based on the amount of SCN^- released upon photoirradiation, which was quantified through the formation of blood-red ($Fe(SCN)^{2+}$) complex after the addition of Fe^{3+} (λ_{max} = 450 nm; ε = 4300 $M^{-1}cm^{-1}$). Reinecke's salt, commercially available as the ammonium salt, was first converted to the potassium salt for use. Specifically, $NH_4[Cr(NH_3)_2(SCN)_4]$ (1 equiv.) was dissolved in warm water, followed by the addition of excess solid potassium nitrate (4 equiv.) to generate a saturated solution of $K[Cr(NH_3)_2(SCN)_4]$. Upon cooling the mixture in an ice bath, the resulting crystals were collected by suction filtration, rinsed with ice-cold water, and dried under vacuum. All steps were performed under dark conditions to prevent photodegradation.

The recommended actinometric procedure was as follows: a freshly prepared 10 mM aqueous solution of $K[Cr(NH_3)_2(SCN)_4]$ was employed to measure the photon flux of 365, 400, 450, 520, and 560 nm LED light. The solution was filtered using a 220 nm syringe filter, and aliquots (100 μL, pH 5.3) were irradiated with LED light at 365, 400, 450, 520, and 560 nm for predetermined durations. An identical, non-irradiated aliquot served as the dark control. Each sample was then mixed with 0.9 mL of a reagent solution containing 0.1 M $Fe(NO_3)_3$ in 0.5 M $HClO_4$. After 5 minutes of incubation in the dark, the mixtures were diluted to a final volume of 2 mL with deionized water, and absorbance was measured at 450 nm. To ensure accuracy, the irradiation time was kept short so that the decomposition did not exceed 10%. The number of photons absorbed per unit time, Nh□/t, was then calculated using the following equations:

$$moles\ SCN^- = \frac{\Delta A_{450\,nm}}{l \times \varepsilon_{450\,nm}} \times 20$$

$$Nh\upsilon/t = \frac{moles\ of\ SCN^-}{\Phi_\lambda \times t \times F}$$

Here $\Delta A_{450\ nm}$ represents the absorbance difference between the irradiated and nonirradiated actinometer solutions; l is the optical path length of the cuvette; $\varepsilon_{450\ nm}$ is the molar extinction coefficient of $Fe(SCN)^{2+}$ at 450 nm (4300 $M^{-1}cm^{-1}$); Φ_λ is the quantum yield of $K[Cr(NH_3)_2(SCN)_4]$ photolysis at a given irradiation wavelength (Φ_{365} = 0.32, Φ_{400} =0.32 , Φ_{450} = 0.31, Φ_{520} = 0.29, Φ_{560} = 0.28); t is the irradiation time; and F is the absorption correction factor, calculated as $F = 1 - 10^{-OD}$, where OD is the absorption value of the $K[Cr(NH_3)_2(SCN)_4]$ solution at the corresponding irradiation wavelength). The amount of **Rh565** generated from the photolysis of **AhCR565** per unit time was determined by UV-Vis spectroscopy of a 10 mM **AhCR565** solution subjected to photoirradiation under the same conditions (wavelength and irradiance) as those used for the photon flux measurements.

Absorption Spectral Deconvolution Method[2]

The UV-Vis absorption spectrum in units of wavelength (nm) was normalized to the molar absorptivity and then converted into the spectrum in unit of wavenumber (cm^{-1}), and then plotted in Origin. The peaks were identified using the "multiple peak fit" function, with the spectrum fitted to a

total of three constituting Gaussian peaks. Specifically, for sharper peaks, the peak centers were assigned a range of ± 500 cm^{-1}, while broader peaks were given a range of ± 2000 cm^{-1}. The peak area was constrained to positive values (>0). If the fitting results reached either the upper or lower boundary even after convergence, the boundary constraints were relaxed.

The fitting results from Origin were copied into a Microsoft Excel spreadsheet. The minimum value of the resulting constituent spectra was determined using the MIN (data range) function in Excel. All data points of the spectra (a1, a2, a3) were adjusted using the function of Value-MIN (data range) + 0.0001, thereby adjusting the baseline such that it starts at 0.0001. These spectra were then plotted with a logarithmic y-axis. Finally, the spectrum was transformed and presented in terms of wavelength (nm). Note: The addition of 0.0001 to each data point ensures positive values for subsequent LOG (value, 10) calculations.

Femtosecond Time Resolved Transient Absorption Spectroscopy

The femtosecond transient absorption (TA) signals were measured with a TA spectrometer (Helios Fire, Ultrafast System). In brief, this system employs a Ti:Sapphire regenerative amplifier (Astrella, Coherent Inc.) as the primary light source. Laser pulses are generated by the amplifier at 800 nm center wavelength with 7 mJ pulse energy and 1 kHz repetition rate. The amplifier output is split into pump and probe branches using a beam splitter. The pump beam is wavelength-tuned through an optical parametric amplifier (OPerA Solo, Coherent Inc.), while the probe beam delivers the remaining beam through a computer-controlled optical delay line before generating a broadband white light continuum (350-700 nm) via nonlinear spectral broadening in a rotating CaF_2 crystal. Spatial and temporal overlap of the two beams is achieved at the sample position within a 2-mm pathlength fused silica cell. A synchronized optical chopper, operating at half the repetition rate (500 Hz), enables alternating acquisition of pump-excited and unexcited probe spectra for differential absorption measurements. The polarization of pump and probe beams are maintained at the magic angle (54.7°) to eliminate anisotropic contributions. The instrument provides an 8-ns temporal detection window, with temporal resolution determined to be 120 ± 10 fs (FWHM). Sample integrity is maintained during measurements via continuous stirring with a magnetic stir bar.

Global fitting is performed using the Glotaran software package[3]. Exponential decay functions are convolved with a Gaussian instrument response function (120 fs FWHM) to account for temporal resolution constraints.

The TA spectra of **AhCR565** (250 μM) in a mixture of MeOH and PBS (50:50, v:v) were obtained using the TA spectrometer, employing a 330 nm pump beam (150 μW). And the spectra were recorded over a time range from 0 to 7.58 ns following 330 nm excitation in a 2 mm quartz cuvette.

HPLC Analysis of Photolysis Products of AhCR565

A 0.5 mM solution of **AhCR565** in MeCN was prepared and irradiated with 365 nm light (50 mW/cm^2) for varying durations. The photolysis products were analyzed using reverse-phase HPLC: t_R = 14.9 minutes, 73% purity (40-95% MeOH/H_2O (containing 0.1% v/v TFA), linear gradient; 25 minutes run; 1 mL/minute flow; detection at 254 nm).

Detection of CO Release from Photolysis of AhCR565 by Gas Chromatography

A 0.5 mM solution of **AhCR565** was prepared in PBS (10 mM, pH = 7.4) containing 40% DMSO. A 2 mL aliquot of this solution was placed in a 10 mL tube, which was connected to a gas

chromatograph. The solution was then irradiated with a 365 nm LED light (95 mW/cm²) for 7 min. The gas released during the photolysis was analyzed using a gas chromatograph (GC2060, Shanghai Ruimin Instrument Co., Ltd.) equipped with a 5A molecular sieve column (2 m length, 3 mm diameter).

The CO release yield from **AhCR565** photolysis was calculated using the following equation. A 6 mL standard CO gas sample (614.73 ppm) served as the reference. Quantitative calculations were performed by comparing the peak area ratios of the reference gas and **AhCR565** under identical conditions. The following formula was applied:

$$Yield\% = \frac{n_{CO}}{n_{AhCR565}} = \frac{\frac{V_{RCO} * 614.73\ ppm * \rho_{CO}}{M_{CO}} * \frac{S_{CO}}{S_{RCO}}}{c_{AhCR565} * V_{AhCR565}}$$

n_{CO} : the molar amount of CO released from **AhCR565**; $n_{\mathbf{AhCR565}}$: the molar amount of CO **AhCR565**; V_{RCO} : the volume of the reference CO gas injected into the detection system. ρ_{CO} : the density of CO; M_{CO} : the molar mass of CO; S_{CO} : the peak area corresponding to CO released from **AhCR565**; S_{RCO} : the peak area of the reference CO gas; $C_{\mathbf{AhCR565}}$: the concentration of the **AhCR565** solution; $V_{\mathbf{AhCR565}}$: the volume of the **AhCR565** solution.

Detection of CO Release from Photolysis of AhCR565 with a fluorescent probe COFP

COPF was synthesized following the procedure outlined in the reference[4]. A mixture solution of **AhCR565** (5 μM), **COPF** (50 μM) and $PdCl_2$ (50 μM) in PBS (10 mM, pH = 7.4, with 1.5% DMSO) was exposed to 520 nm light (30 mW/cm^2). And the fluorescence emission spectra (λ_{ex} = 490 nm) were recorded at various irradiation intervals.

NO Quantification Using the Fluorescent Probe DAN

DAN (2,3-diaminonaphthalene), a commercial NO fluorescent probe, reacts with NO to produce NAT in the presence of oxygen. The following solutions were prepared:

- Reagent A: A 0.62 M hydrochloric acid solution containing 0.025 mg/mL DAN.
- Reagent B: A 1.5 M hydrochloric acid solution.
- Reagent C: A 3 M sodium hydroxide solution.
- Reagent D: A 2 mM sodium nitrite solution.

A calibration curve was constructed using sodium nitrite standards, with linearity observed within the detection range. Sodium nitrite solutions with varying concentrations (1800, 1500, 1200, 900, 600, 400, 200, 100, 50, 25, 12.5 μM) were prepared by diluting reagent D with deionized water. The DAN reagent was prepared by mixing 1 mL of reagent A and 1 mL of reagent B, then adding 10 μL of sodium nitrite solution at varying concentrations for a 5-minute reaction. Afterward, 1 mL of reagent C was added, and the reaction continued for 1 minute. The calibration curve for NO detection was determined as: $y = 33.643x + 9.584$ ($R^2 = 0.999$), where y is fluorescence intensity and x is the concentration of sodium nitrite (μM).

To quantify NO released during the photolysis of **AhCR565**, 3 μL of a **AhCR565** DMSO solution (5 mM) was added to 2 mL of DAN reagent and irradiated with a 520 nm light (30 mW/cm^2) for the specified time. The reaction was then continued in the dark for 5 minutes. After adding 1 mL of reagent C and allowing it to react for 1 minute, the fluorescence emission spectrum was recorded.

Radical Trapping and Electron Paramagnetic Resonance (EPR) Studies

EPR spectra were recorded on a on Bruker EMX instrument EMXPLUS-10/12 (Bruker

Analystische Messtechnick GMBH, Germany). The spectra were measured at 298 K. Typical instrumental conditions were as follows: central field, 3506.7 G; modulation frequency, 100 kHz; modulation amplitude, 1.00 G; sweep width, 100 G; microwave power, 2 mW; sweep time, 60.0 s; conversion time, 58.60 ms; time constant, 0 ms.

1) NO Trapping with PTIO

2-Phenyl-4,4,5,5-tetramethylimidazoline-1-oxyl-3-oxide (PTIO) was used as a spin capture agent for nitric oxide (NO). An aqueous solution (containing 10% DMSO) of PTIO (20 μM) and **AhCR565** (20 μM) was irradiated with 520 nm light (36 mW/cm²) for 20 minutes. EPR data was then collected to analyze the NO adduct.

2) Radical Trapping with DMPO

5,5-Dimethyl-1-pyrroline *N*-oxide (DMPO) was employed as a radical trapping agent. A mixture of DMPO (10 mM) and **AhCR565** (1 mM) in acetonitrile were irradiated with a white LED light (LOT-Quantum Design GmbH) for 2.5, 5, and 7.5 minutes before data acquisition.

Cell Culture

L929 cells were purchased from Cell Bank of Type Culture Collection of Chinese Academy of Sciences. L929 cells were all maintained in Dulbecco's Modified Eagle Medium (DMEM, Gibco) supplemented with 10% fetal bovine serum (FBS, KEL Biotech) and 2% penicillin-streptomycin (10,000 U/mL). The cells were cultured in a humidified atmosphere of 5% CO_2/95% air at 37 °C and grown on 100 mm cell culture dish (Labselect, 12311) for 1–2 days to reach 70–90% confluency before use.

Confocal fluorescence imaging and colocalization analysis

L929 cells were seeded at a density of 1×10^5 cells/mL in 10-mm glass-bottom confocal dishes (iCell) with a 1-mL seeding volume, one day prior to imaging. After overnight incubation, the medium was removed, and cells were incubated with **AhCR565** (5 μM) for 60 minutes, washed with PBS for 3 times, and then placed in fresh DMEM. Fluorescence microscopy was conducted using an Olympus confocal microscope with a 60× oil-immersion objective lens after cells were irradiated with the built-in 561 nm laser for various time (λ_{ex}=561 nm, λ_{em}=570-620 nm).

L929 cells were incubated with a mitochondrial (Mito Tracker™ Deep Red FM, 20 nM) or lysosome-targeting probe (LysoTracker Deep Red, 20 nM) for 30 minutes, followed by washing with PBS three times. The cells were then incubated with **AhCR565** (2 μM) for 60 minutes, washed with PBS three times, and placed in fresh DMEM. After photoirradiation using a built-in 561 nm laser for 2 minutes, fluorescence images were collected from the green channel (**AhCR565**, λ_{ex} = 561 nm, λ_{em} = 570-620 nm) and the red channel (Mito Tracker™ Deep Red FM or LysoTracker Deep Red, λ_{ex} = 640 nm, λ_{em} = 650-750 nm), respectively.

Intracellular CO and NO Imaging

L929 cells were incubated with COFP (2 μM) and $PdCl_2$ (4 μM), or DAF-FM-DA (2 μM, Beyotime) with or without PTIO (10 μM) for 30 minutes, washed with PBS, and then incubated with **AhCR565** (2 μM) for 60 minutes. Following another wash with PBS, cells were irradiated with 520 nm light (20 mW/cm²) for 15 minutes, and then incubated for an additional 30 minutes. Finally, fluorescence images were captured to visualize intracellular CO and NO. For COPF or DAF-FM-DA, λ_{ex} = 488 nm, λ_{em} = 520-540 nm.

Cell Viability Assessment

Cell viability was assessed using a Cell Counting Kit-8 (CCK-8, TargetMol) following the manufacturer's instructions.

Dark Cytotoxicity: L929 cells (8×10^3 cells per well) were seeded in 96-well plates and incubated for 24 hours. Cells were then treated with different concentrations of **AhCR565** (0, 1, 2, 5, 10, 15, 20, 30 μM) for 24 hours.

Photo-Cytotoxicity: L929 cells were incubated with different concentrations of **AhCR565** for 12 hours, followed by exposure to a 520 nm light source (20 mW/cm²) for 30 minutes. The cells were then cultured for another 12 hours. Afterward, 100 μL of DMEM medium containing 10 μL of CCK-8 reagent was added to each well and incubated at 37 °C for 1 hour. The absorbance at 450 nm was measured by a microplate reader.

***In Vitro* Antibacterial Test**

Methicillin-resistant *Staphylococcus aureus* (MRSA, USA300LAC) was cultured in 2 mL of Luria–Bertani (LB) medium at 37 ℃ with constant stirring for 18 hours. The bacterial suspension was then adjusted to a concentration of 10^6 CFU/mL using LB medium. Six experimental groups were established: blank control, **AhCR565** + hv, **AhCR565** - hv, NOD + hv, NOD - hv, and CORM-3.

96-well plates were prepared, with each well containing 100 μL of bacterial culture and 100 μL of LB medium with varying concentrations of the tested compounds. For the light-exposed groups, samples were irradiated with 520 nm light (20 mW/cm²) for 30 minutes and incubated for another 8 hours. Finally, the absorbance at 600 nm (OD_{600}) was measured using a microplate reader.

Scanning Electron Microscopy (SEM) of MRSA

The bacteria (1×10^7 CFU/mL) were incubated with 10 μM **AhCR565** for 1 hour, followed by exposure to dark or light (20 mW/cm²) for 30 min. Then, the bacteria were fixed with 2.5% glutaraldehyde overnight at 4 °C. After washing with sterile PBS, the bacteria were dehydrated through a graded ethanol series (30%, 50%, 70%, 80%, 90%, and 100%) for 15 minutes at each concentration. The ethanol was then replaced with the mixture of tert-butanol and ethanol (1:1), and next pure tert-butanol. A 10 μL sample was placed on a silicon wafer and freeze-dried. The morphological characteristics of the bacteria were observed using a scanning electron microscope.

Antimicrobial Study *In Vivo*

Development and Treatment Protocol of Skin Wound Infection Mouse Model

An infection model was established in BALB/c mice (5-6 weeks old). The backs of the mice were shaved, and full-thickness skin wounds (6 mm in diameter) were created. A 10 μL PBS suspension of MRSA (1×10^8 CFU/mL) was applied to the wound site. After 6 hours of infection, the infected wounds were treated with 10 μL of **AhCR565** (5 mg/mL in a mixture of sterilized water with 10% (v/v) Solutol HS-15 and 10% (v/v) DMSO), CORM-3 (10 mg/mL in sterilized water with 10% (v/v) solutol HS-15 and 10% (v/v) DMSO), **NOD** (5 mg/mL in a mixture of sterilized water with 10% (v/v) solutol HS-15 and 10% (v/v) DMSO), **Rh565** (5 mg/mL in a mixture of sterilized water with 10% (v/v) solutol HS-15 and 10% (v/v) DMSO), vancomycin (48.75 μg/mL in sterilized water), or PBS (10 mM, pH 7.4). The process of irradiation was conducted by a 520 nm LED (20 mW/cm²) and continuously irradiated for 20 minutes. The same treatment was administered every 48 hours from

days 1 to 9. All animal experimental procedures were approved by the Institutional Animal Care and Use Committee (IACUC) of East China Normal University (m20240904).

Bacterial Plating and Counting

On days 1, 3, 5, and 7, infected tissues were excised, weighed, and homogenized with an appropriate volume of normal saline. The homogenates were plated on agar and cultured overnight at 37°C. Colony-forming unit (CFU) counts were performed to determine bacterial load.

Hematoxylin and Eosin (HE) Staining

On days 3 and 7, mice from each group were euthanized. The wound and surrounding tissues were collected and fixed in 4% paraformaldehyde overnight. The tissues were then dehydrated, trimmed, and embedded in paraffin. Skin sections, 3-4 μm thick, were prepared using a Leica RM2016 pathological microtome. The sections were stained with hematoxylin and eosin (HE) and imaged using an optical microscope. Images were captured at 20× magnification to evaluate wound healing and inflammatory infiltration in each group. Histological analyses were conducted on at least three independent wounds per group, with the images presented being representative of all replicates.

Sirius Red Staining

Skin sections were prepared using the same method as described previously, stained with Sirius red, and imaged using an optical microscope. Images were captured at 20× magnification to assess collagen deposition in the wound tissue. Collagen fibers appeared red, while muscle fibers appeared yellow. Histological analyses were conducted on at least three independent wounds per group, with the images presented being representative of all replicates.

CD31 Immunofluorescence Staining

Paraffin sections were deparaffinized and rehydrated prior to staining. The sections were blocked with 3% (w/v) bovine serum albumin (BSA) for 30 minutes. Subsequently, the primary antibody was applied and incubated at 4 °C overnight. After thorough washing with PBS for 15 minutes, a secondary antibody conjugated to Alexa Fluor® 488 Goat Anti-Rabbit IgG was added and incubated for 50 minutes to label the antigen. The sections were then sealed and stored at 4 °C in the dark before imaging. Observations were performed at 20× magnification using an Olympus FV3000 system (λ_{ex} = 488 nm, λ_{em} = 517–537 nm). Histological analyses were conducted on at least three independent wounds per group, and the images presented are representative of all replicates.

Statistical Analysis

Data are presented as mean ± S.D., with 3-6 samples per experimental group. The normality of the data was first assessed, followed by analysis using the Student's t-test. Statistical significance was set at $p < 0.05$ (*); $P < 0.01$ (**); $P < 0.001$ (***).

Synthetic procedures and Compound Characterization

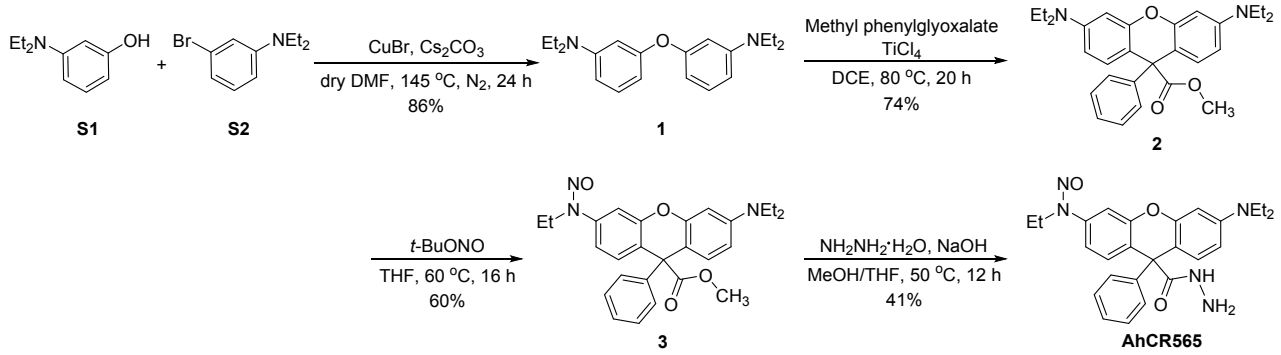

Scheme S1. Synthesis of Compound AhCR565

Synthesis of 3,3'-oxybis(*N,N*-diethylaniline) (1)

3-(diethylamino)phenol (**S1**, 10.86 g, 65.75 mmol, 1.50 equiv), 3-bromo-*N,N*-diethylaniline (**S2**, 10.00 g, 43.83 mmol, 1.00 equiv), Cs_2CO_3 (21.42 g, 65.75 mmol, 1.50 equiv) and dry DMF (50 mL) were added to a 250-mL flask. The mixture was stirred and purged with argon for 15 min before CuBr (628.80 mg, 4.38 mmol, 0.10 equiv) was added. The reaction was purged with argon for another 15 min. Then, the reaction was heated at 145 ℃ for 24 h before cooled to room temperature. The reaction mixture was filtered through Celite and concentrated under reduced pressure. The mixture was extracted by DCM. The combined organic layers were dried over Na_2SO_4 and concentrated under reduced pressure. The crude product was purified by column chromatography (PE:EA = 200:1) to yield **1**[5] (11.83 g, 86%) as yellow oil.

^{1}H NMR (600 MHz, $CDCl_3$) δ 7.12 (t, *J* = 8.0 Hz, 2H), 6.41 (dd, *J* = 9.3, 2.1 Hz, 4H), 6.29 – 6.26 (m, 2H), 3.33 (q, *J* = 7.1 Hz, 8H), 1.15 (t, *J* = 7.1 Hz, 12H).

Synthesis of methyl 3,6-bis(diethylamino)-9-phenyl-9*H*-xanthene-9-carboxylate (2)

To a stirred solution of 3,3'-oxybis(*N,N*-diethylaniline) (**1**, 3.80 g, 12.16 mmol, 1.00 equiv.), methyl 2-oxo-2-phenylacetate (2.00 g, 12.16 mmol, 1.00 equiv.) in 100 mL anhydrous DCE was added $TiCl_4$ (1.47 ml, 13.38 mmol, 1.10 equiv.). The mixture was heated to 80 ℃ under N_2 for 20 hours. After cooling, the solution was neutralized with saturated aqueous $NaHCO_3$ and concentrated under reduced pressure. The residue was extracted with DCM and H_2O. The combined organic layers were dried over Na_2SO_4 and concentrated under reduced pressure. The crude product was purified by column chromatography (PE:EA = 30:1 to 20:1, v/v) to yield **2**[6] (4.15 g, 74%) as a yellow solid.

^{1}H NMR (600 MHz, $CDCl_3$) δ 7.28 (dd, *J* = 8.4, 6.7 Hz, 2H), 7.26 – 7.24 (m, 2H), 7.23 – 7.19 (m, 1H), 6.84 (d, *J* = 8.8 Hz, 2H), 6.36 (d, *J* = 2.7 Hz, 2H), 6.33 (dd, *J* = 8.8, 2.7 Hz, 2H), 3.71 (s, 3H), 3.34 (q, *J* = 7.1 Hz, 8H), 1.17 (t, *J* = 7.1 Hz, 12H).

Synthesis of methyl 3-(diethylamino)-6-(ethyl(nitroso)amino)-9-phenyl-9*H*-xanthene-9-carboxylate (3)

To a stirred solution of compound **2** (3.00 g, 6.54 mmol, 1.00 equiv.) in 100 mL THF was added *t*-BuONO (1.56 mL, 13.08 mmol, 2.00 equiv.). The mixture was stirred at 60 ℃ for 16 hours. After the reaction was complete, the THF was removed under vacuum. The residue was extracted by DCM and H_2O, and the combined organic layers were dried over Na_2SO_4 and concentrated under reduced

pressure. The crude product was purified by column chromatography (PE:EA = 20:1 - 15:1, v/v) to yield **3** (1.81 g, 60%) as a yellow solid.

^{1}H NMR (600 MHz, $CDCl_3$) δ 7.32 (t, *J* = 7.5 Hz, 2H), 7.29 (d, *J* = 2.4 Hz, 1H), 7.27 (d, *J* = 1.2 Hz, 1H), 7.25 (d, *J* = 6.9 Hz, 2H), 7.20 (dd, *J* = 8.6, 2.4 Hz, 1H), 7.09 (d, *J* = 8.6 Hz, 1H), 6.87 (d, *J* = 9.6 Hz, 1H), 6.38 (dd, *J* = 4.7, 2.3 Hz, 2H), 4.05 (q, *J* = 7.2 Hz, 2H), 3.74 (s, 3H), 3.35 (q, *J* = 7.1 Hz, 4H), 1.18 (t, *J* = 7.0 Hz, 9H).

^{13}C NMR (151 MHz, $CDCl_3$) δ 173.57, 151.57, 151.54, 148.44, 144.97, 141.33, 132.36, 131.71, 129.21, 128.17, 126.94, 123.13, 113.02, 109.54, 107.84, 106.54, 97.60, 55.51, 52.99, 44.35, 38.90, 12.66, 11.77.

ESI-HRMS [$C_{27}H_{29}N_3O_4$ + Na^+] calc. 482.2056, found 482.2055.

Synthesis of *N*-(6-(diethylamino)-9-(hydrazinecarbonyl)-9-phenyl-9*H*-xanthen-3-yl)-*N*-ethylnitrous amide (AhCR565)

To a stirred solution of NaOH (2.06 g, 51.41 mmol, 25.00 equiv.) in 50 mL MeOH was added hydrazine hydrate (5 mL, 102.82 mmol, 50.00 equiv.). The mixture was stirred at room temperature for 20 minutes. Then compound **3** (945 mg, 2.06 mmol) in 50 mL THF was added to the reaction mixture, which was heated to 50°C for 12 hours. After completion of the reaction, the solution was neutralized with 3 M HCl. Then the mixture was extracted by DCM and H_2O. The combined organic layers were dried over Na_2SO_4 and concentrated under reduced pressure. The crude product was purified by column chromatography (DCM) to yield **AhCR565** (387 mg, 41%) as a yellow solid.

^{1}H NMR (600 MHz, $CDCl_3$) δ 7.35 – 7.31 (m, 3H), 7.30 – 7.27 (m, 3H), 7.24 (d, *J* = 8.6 Hz, 1H), 7.21 (dd, *J* = 8.6, 2.3 Hz, 1H), 6.97 (s, 1H), 6.67 (d, *J* = 8.8 Hz, 1H), 6.40 (d, *J* = 2.7 Hz, 1H), 6.35 (dd, *J* = 8.8, 2.7 Hz, 1H), 4.05 (q, *J* = 7.1 Hz, 2H), 3.92 (s, 2H), 3.35 (q, *J* = 7.0 Hz, 4H), 1.18 (td, *J* = 7.1, 1.9 Hz, 9H).

^{13}C NMR (151 MHz, $CDCl_3$) δ 173.20, 151.84, 148.76, 144.71, 141.65, 132.79, 130.96, 129.69, 128.24, 126.97, 123.36, 113.32, 108.98, 108.18, 106.46, 98.12, 54.93, 44.40, 38.85, 12.58, 11.77.

ESI-HRMS [$C_{26}H_{29}N_5O_3$ + Na^+] calc. 482.2168, found 482.2162.

Table S1. Summary of wavelength-dependent photochemical transformation from **AhCR565** to **Rh565**. Note, f specifically refers to the quantum yield for the photoconversion of **AhCR565** to **Rh565** upon light irradiation, and values are expressed as mean ± SD (n = 3).

Wavelength-dependent photochemical transformation from AhCR565 to Rh565					
λ (nm)	365	400	450	520	560
Φ (%)	4.053±0.116	3.664±0.021	0.346±0.004	0.087±0.017	0.038±0.004
ε ($cm^{-1}M^{-1}$)	5770±216	4070±102	1940±95	1330±64	992±49
Φ × ε	233.9	149.1	6.712	1.157	0.377

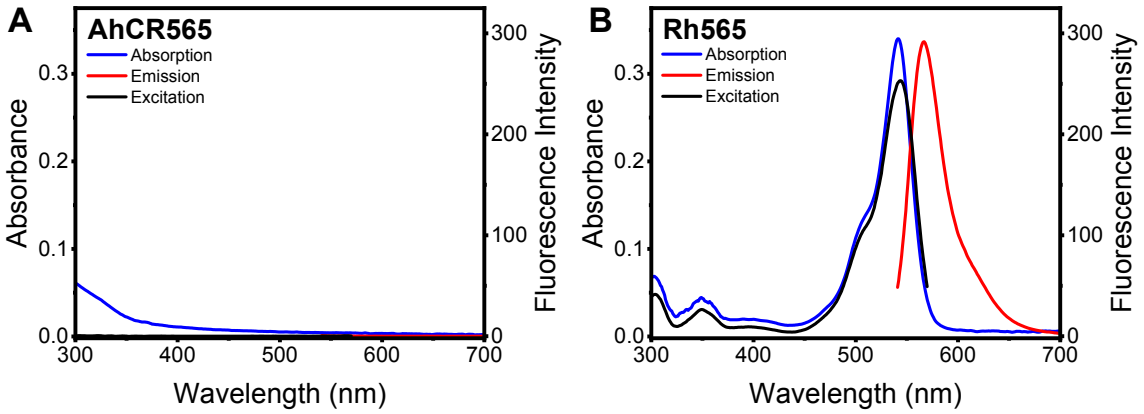

Figure S1. UV-Vis absorption, excitation and fluorescence emission spectra of (A) **AhCR565** (5 μM) and (B) **Rh565** (5 μM) in PBS (10 mM, pH = 7.4, with 0.5% DMSO).

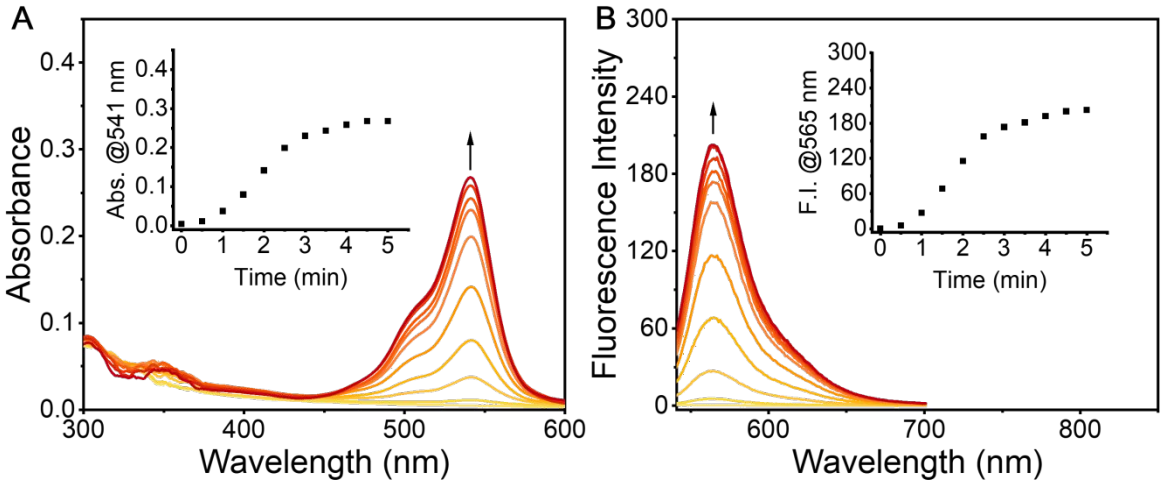

Figure S2. (A) UV-Vis absorption and (B) fluorescence emission spectral changes of **AhCR565** (5 μM) in PBS (10 mM, pH = 7.4, with 0.5% DMSO) under irradiation with white light (1W). Inset: Time-dependent changes in absorbance @541 nm or fluorescence intensity (λ_{ex} = 541 nm) @565 nm during irradiation.

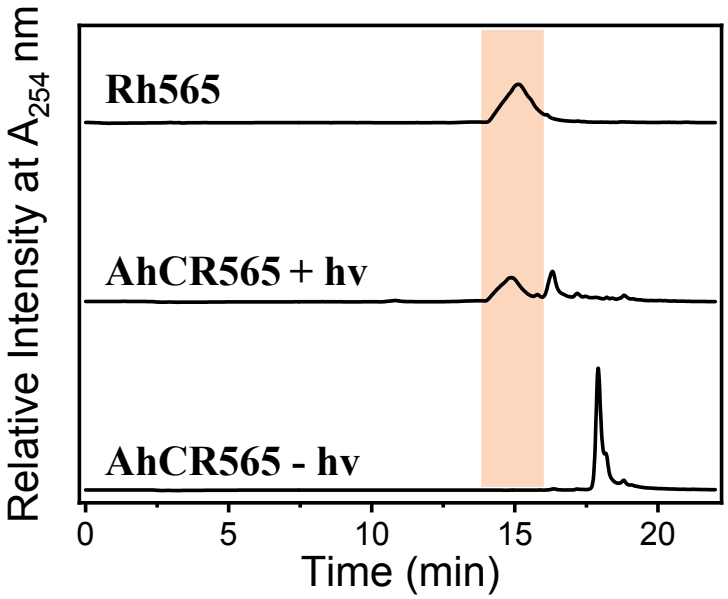

Figure S3. HPLC traces of **Rh565** (0.5 mM) and **AhCR565** (0.5 mM) in MeCN before and after 3 minutes of irradiation with a 365 nm LED (50 mW/cm^2).

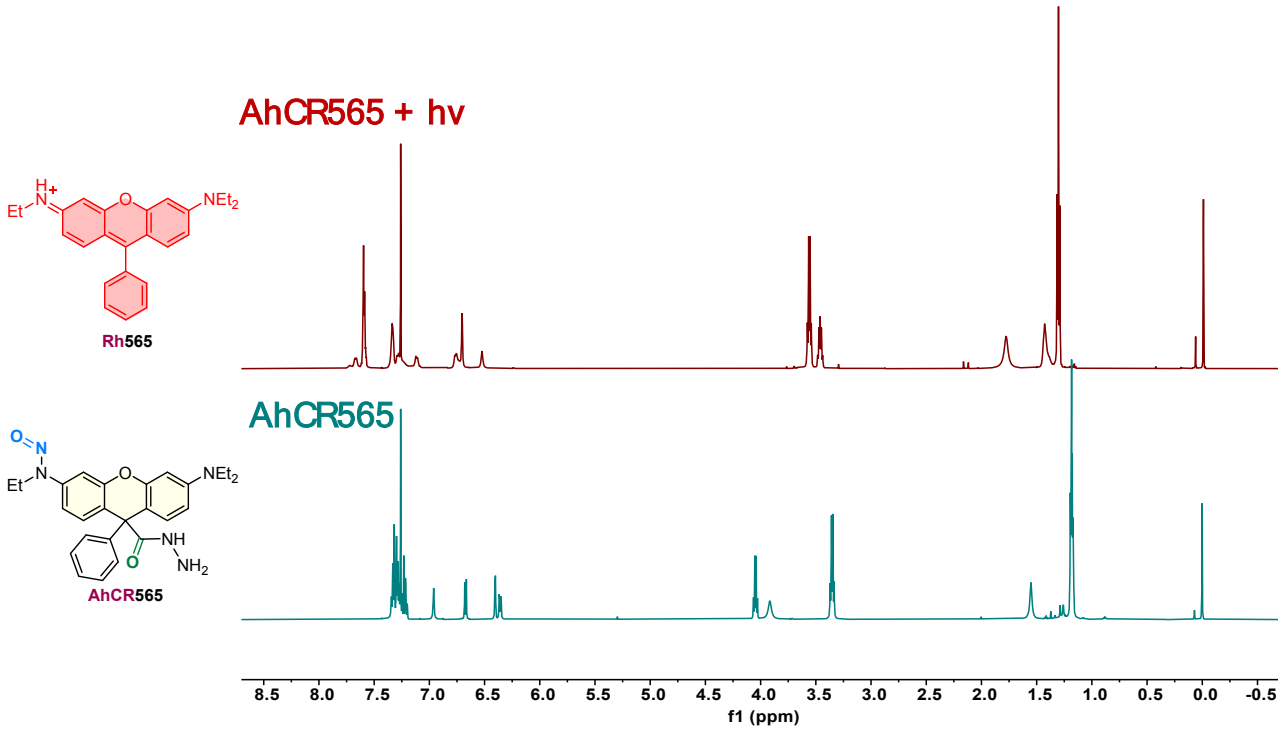

Figure S4. Confirmation of the photolysis product of **AhCR565** as **Rh565** by ^{1}H NMR.

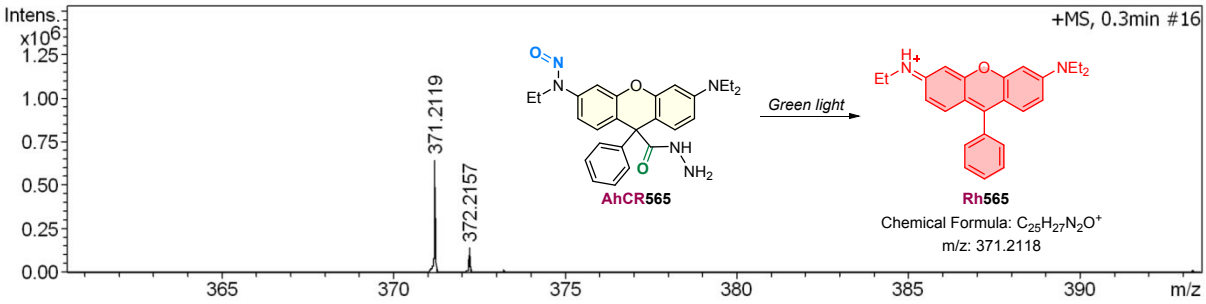

#	m/z	Res.	S/N	I	I %	FWHM
1	371.2119	28123	1015.3	643788	100.0	0.0132
2	372.2157	20154	221.5	140256	21.8	0.0185
3	373.2209	14563	23.0	14532	2.3	0.0256

Meas. m/z	#	Ion Formula	m/z	err [ppm]	mSigma		Score	rdb	e¯ Conf	N-Rule
371.2119	1	C25H27N2O	371.2118	-0.2	32.9	4	100.00	13.5	even	ok

Figure S5. Confirmation of the photolysis product of **AhCR565** as **Rh565** by mass spectra.

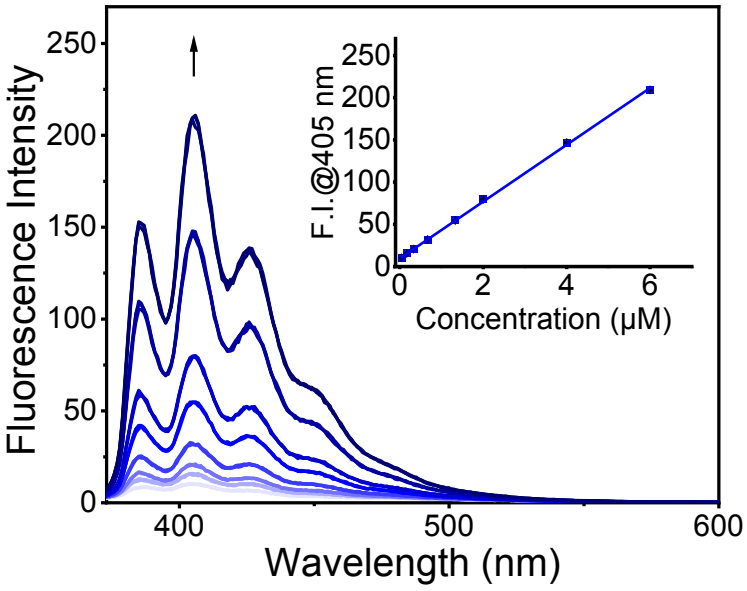

Figure S6. The titration curve of DAN (53 μM) with sodium nitrite.

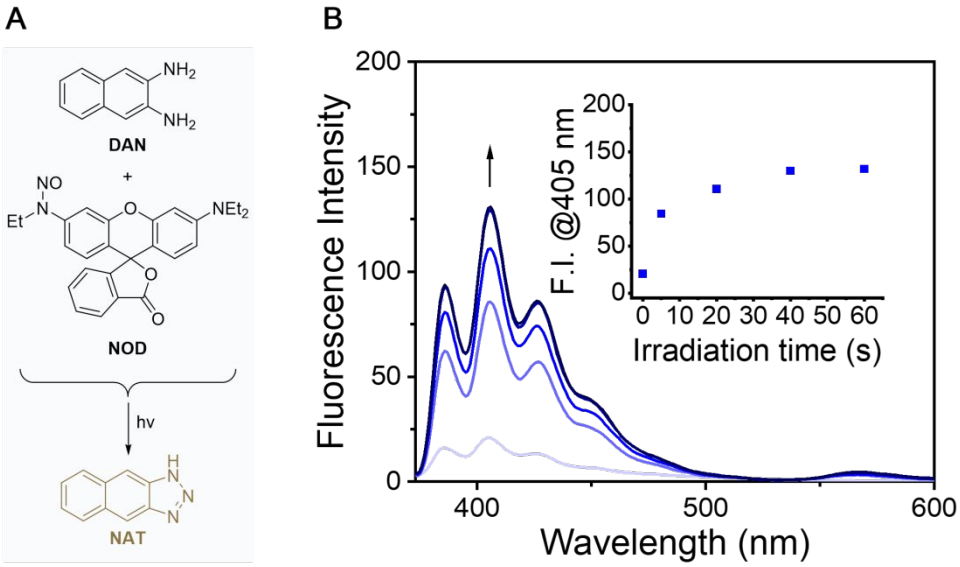

Figure S7. Fluorescence emission spectral changes of a mixture of **NOD** (5 μM) and DAN (53 μM) under 520 nm LED irradiation (30 mW/cm²). The NO release yield of NOD was quantitatively determined to be 72.8 ± 0.7 %.

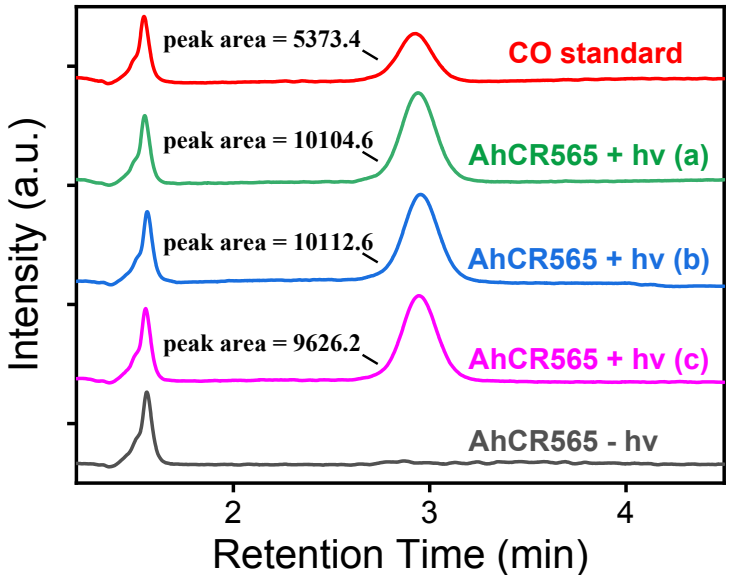

Figure S8. Quantitative analysis of CO release from **AhCR565** by GC by three independent experiments.

Calculation example:

$$Yield\% = \frac{\frac{6\ mL * 614.73 * 10\text{^}(-6) * 1.25\ mg/mL}{28\ g/mol} * \frac{10104.6}{5373.4}}{0.002\ L * 0.5\ mmol/L}$$

$$Yield\% = 30.9\%$$

Based on the calculation formula, the CO release efficiencies were determined to be 30.9%, 31.0%, and 29.5% in three independent measurements. Accordingly, the final result was calculated to be 30.5% ± 0.9% (n = 3).

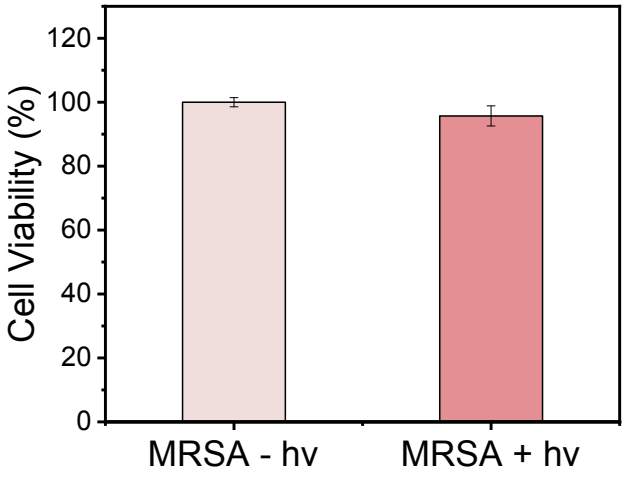

Figure S9. Bacterial viability of MRSA following 30 minutes of 520 nm light irradiation at 20 mW/cm².

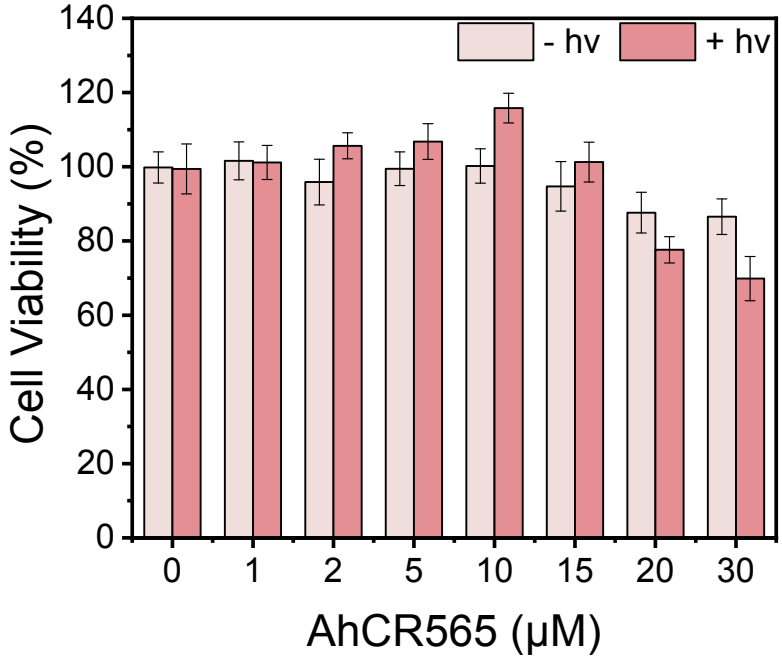

Figure S10. The viability of L929 fibroblast cells treated with **AhCR565** at varying concentrations evaluated using the CCK-8 assay under both dark and light irradiation conditions (520 nm, 20 mW/cm² for 30 minutes).

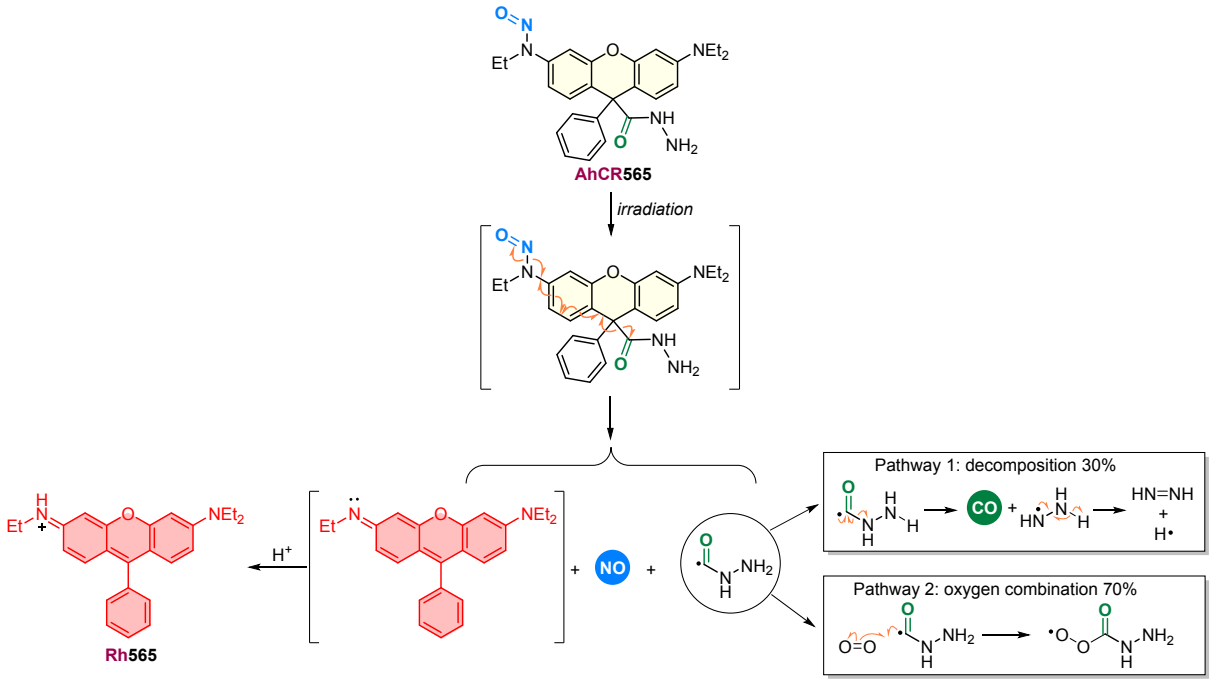

Scheme S2. Proposed photolysis pathway of **AhCR565** under 520 nm LED light irradiation, highlighting both the primary decomposition mechanism and the possible side reaction pathway in the presence of oxygen.

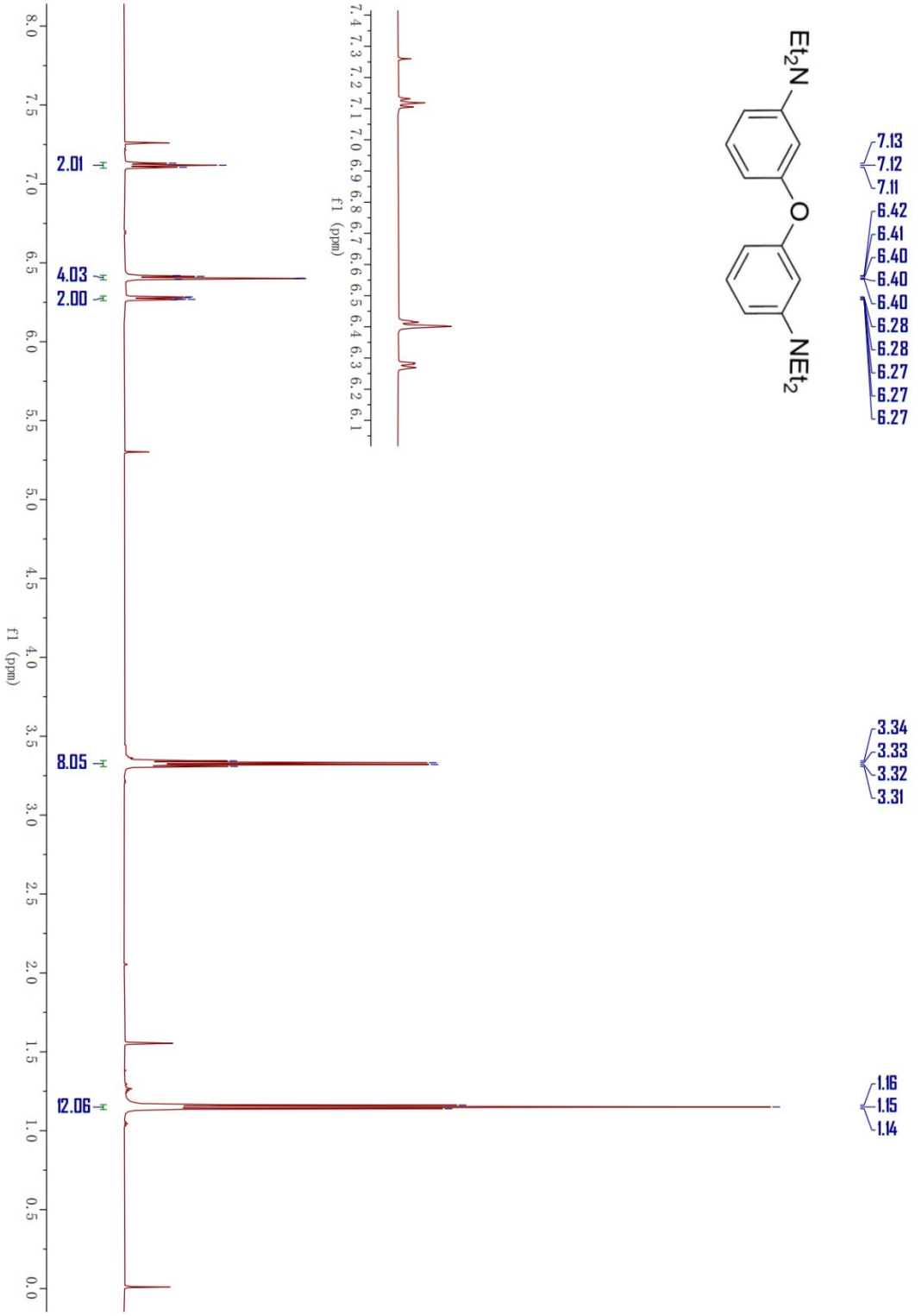

Figure S11. ^{1}H NMR of compound **1** in $CDCl_3$ (600 MHz).

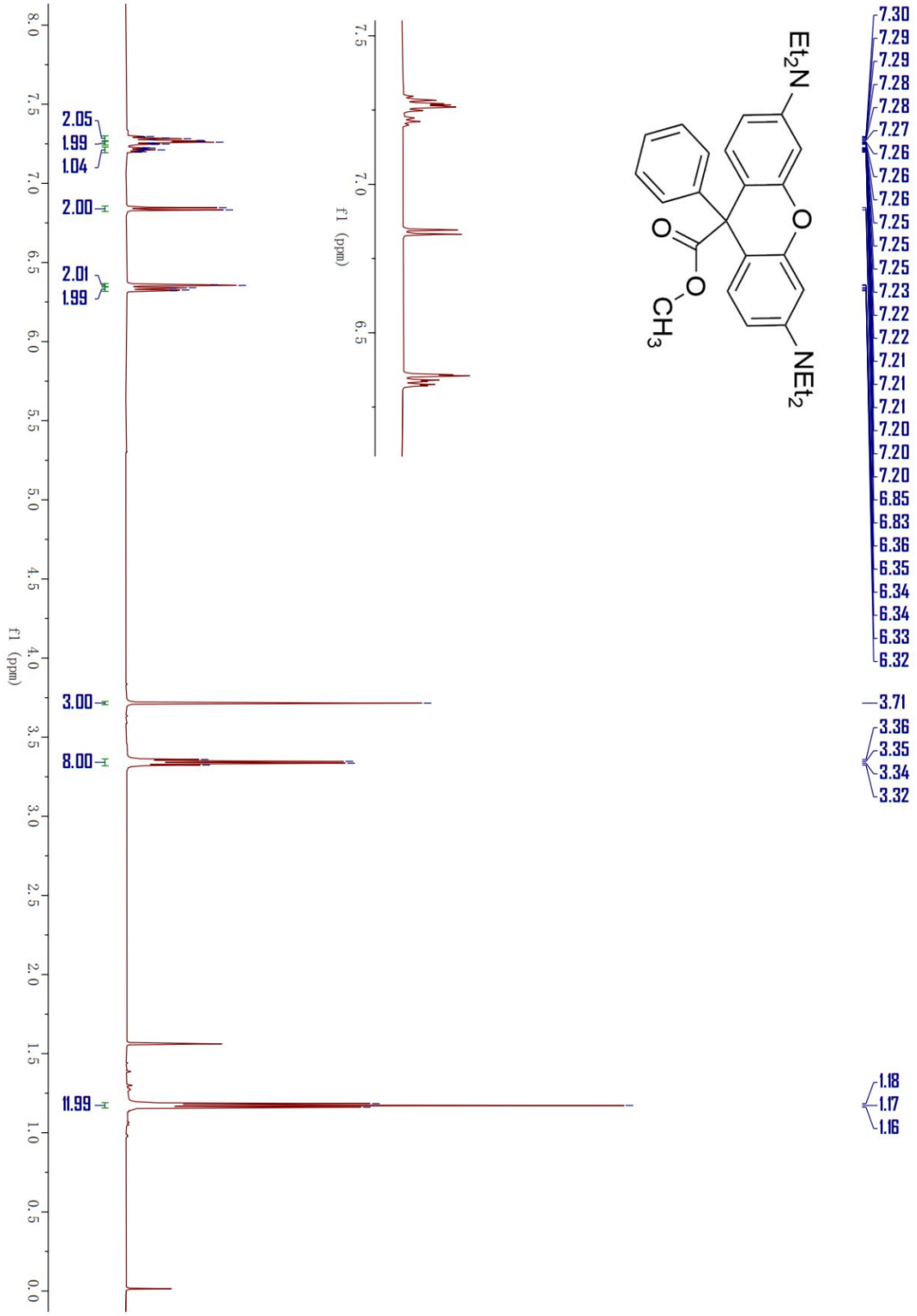

Figure S12. ^{1}H NMR of compound **2** in $CDCl_3$ (600 MHz).

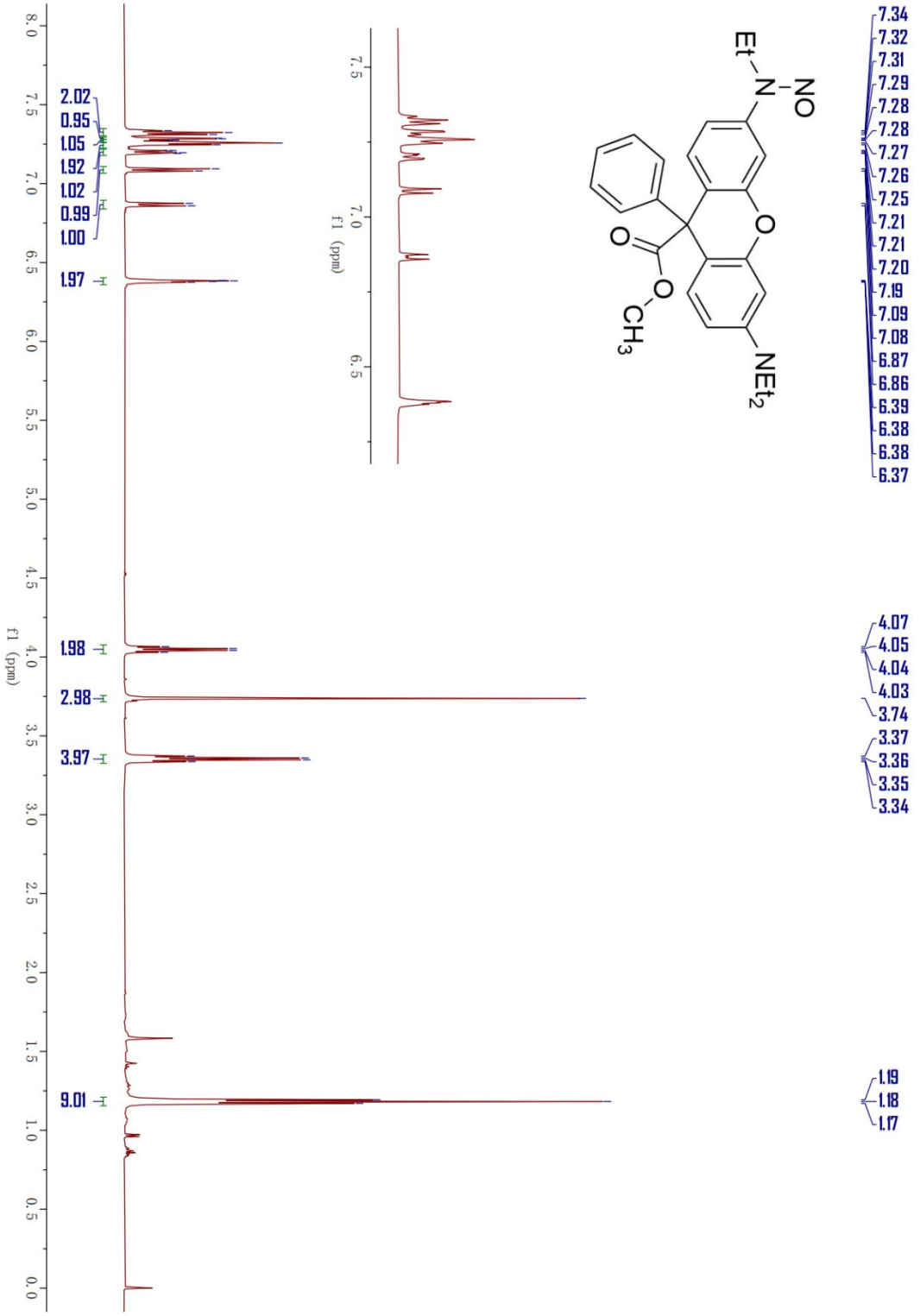

Figure S13. ^{1}H NMR of compound **3** in $CDCl_3$ (600 MHz).

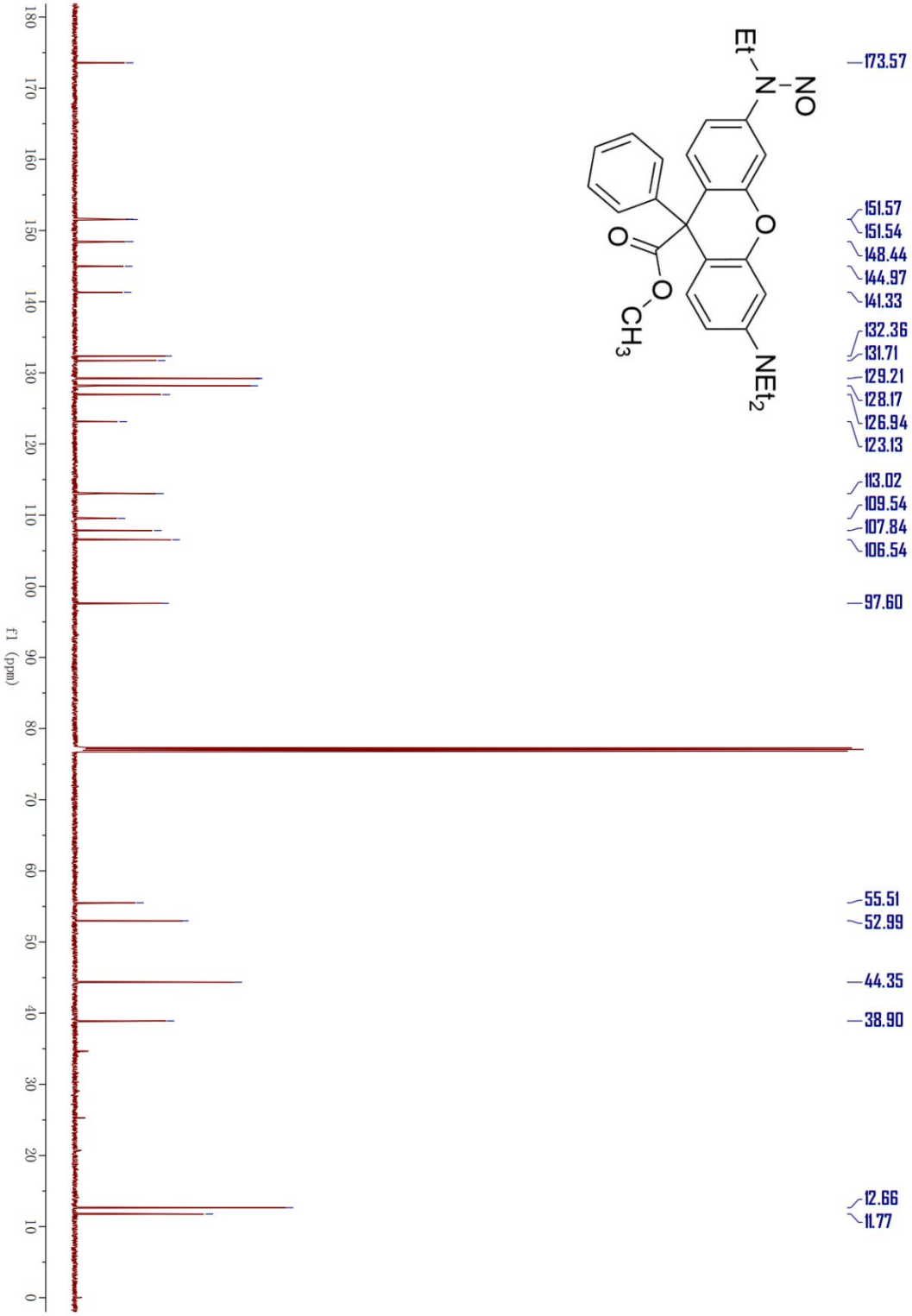

Figure S14. ^{13}C-NMR of compound **3** in $CDCl_3$ (151 MHz).

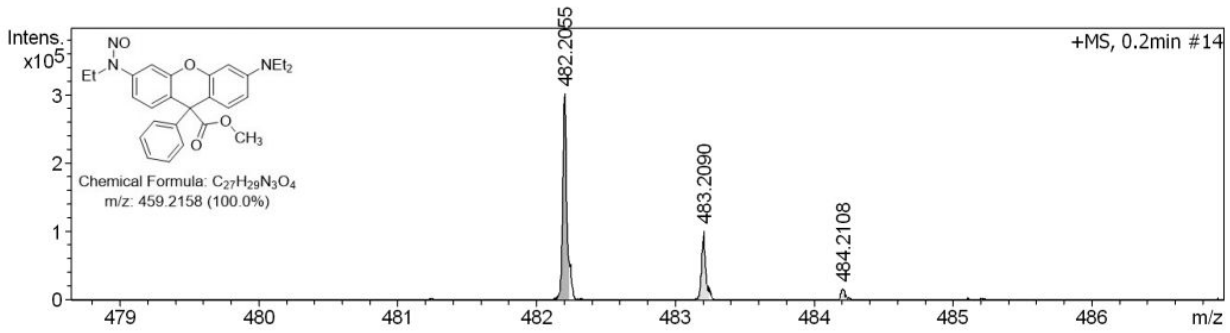

Figure S15. HRMS of compound **3**.

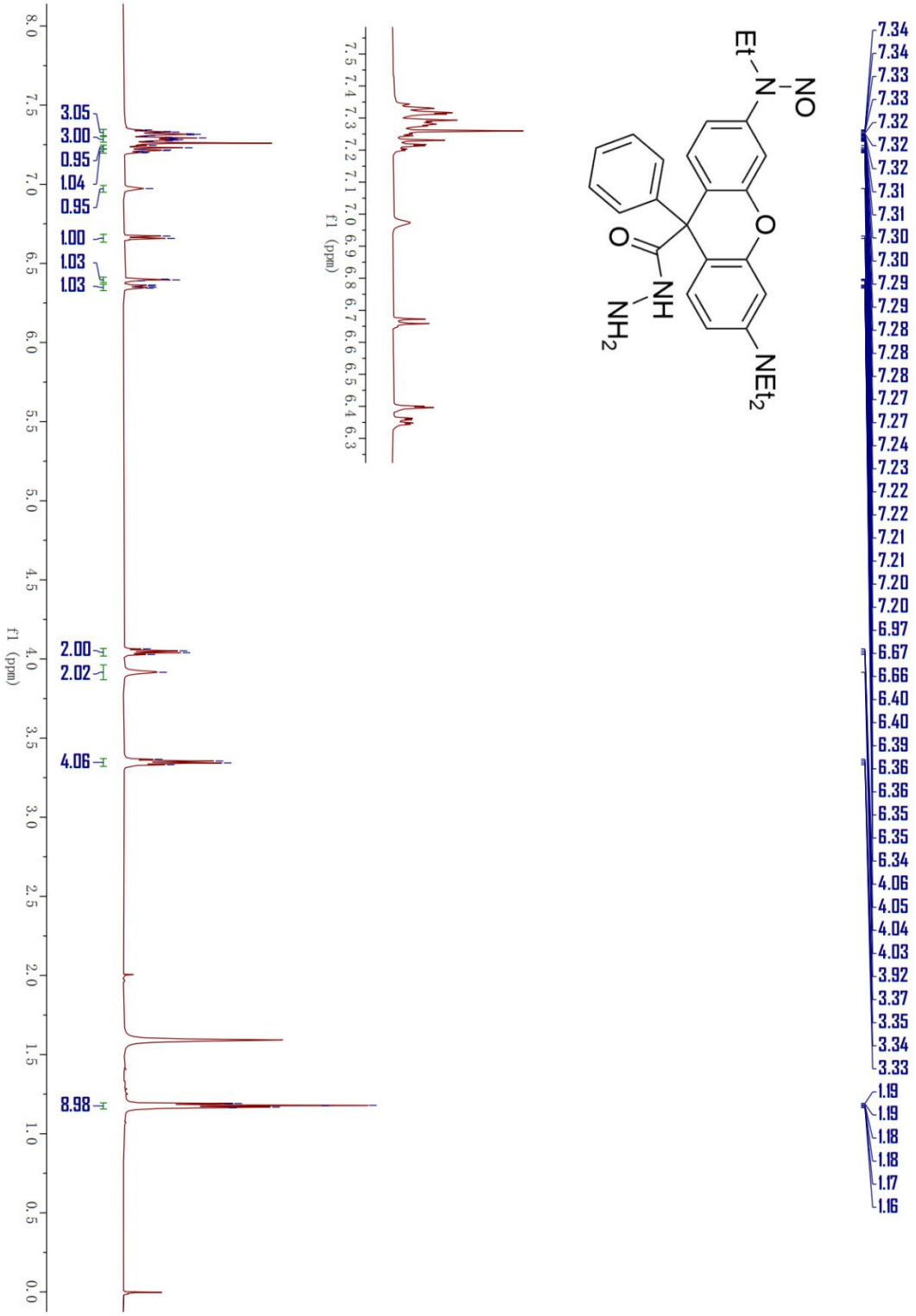

Figure S16. ^{1}H NMR of compound **AhCR565** in $CDCl_3$ (600 MHz).

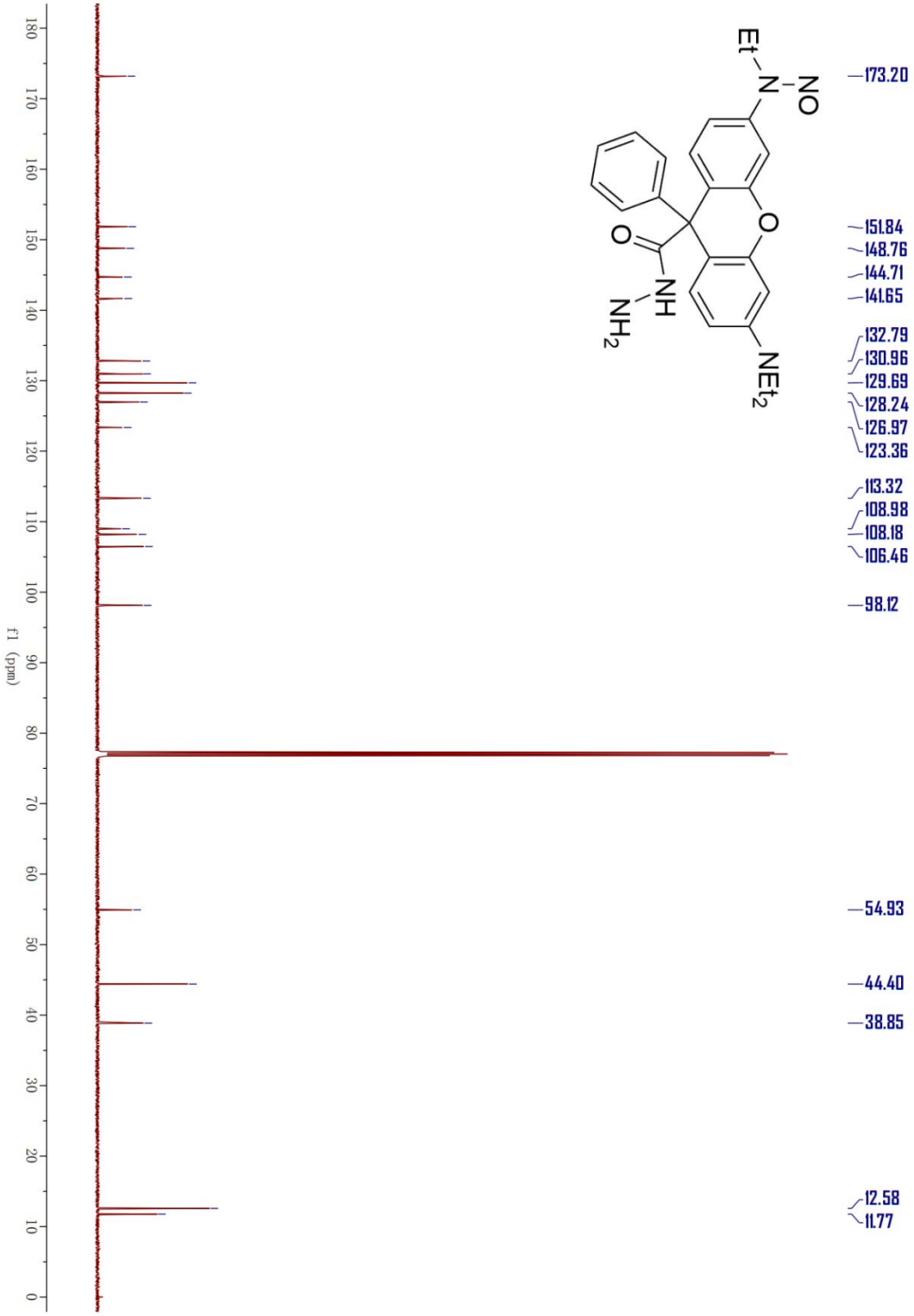

Figure S17. ^{13}C NMR of compound **AhCR565** in $CDCl_3$ (151 MHz).

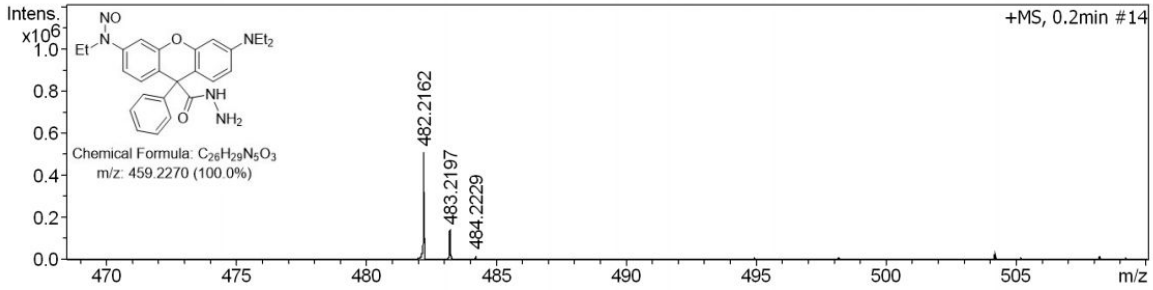

Figure S18. HRMS of compound **AhCR565**.

Additional Discussion

Currently, existing NO and CO co-release systems can be broadly classified into two categories.

The first category primarily relies on formulations that encapsulate separate NO and CO donors. Representative examples include:

A. Yang et al. incorporated $Ru(CO)_3Cl$(glycinate) (CORM-3) and *S*-nitrosoglutathione (GSNO) into a hydrogel patch as CO and NO donors, respectively (*Nat. Commun.* **2023**, *14*, 2417).
B. Wang et al. co-loaded *N,N*′-Di-sec-butyl-*N,N*′-dinitroso-1,4-phenylenediamine (BNN, an NO donor) and manganese carbonyl (CORM-1, a CO donor) into upconversion nanoparticles (*Chem. Eng. J.* **2024**, *480*, 147850).
C. Xu and Zhang et al. employed GSNO and a manganese carbonyl complex (CORM) within upconversion nanoparticles for dual gas release (*ACS Appl. Mater. Interfaces* **2023**, *15*, 56796–56806; *ACS Appl. Bio Mater.* **2024**, *7*, 7585–7594).
D. Hu et al. constructed micelles via co-assembly of PHFP and PTFNOP copolymers, using 3-hydroxyflavone (3-HF) as the CO donor and *N*-nitrosobenzenamine as the NO donor (*Angew. Chem. Int. Ed.* **2025**, *64*, e202419939).

These systems rely on co-loaded NO and CO donors that often **exhibit distinct release mechanisms and kinetics**, **resulting in asynchronous gas release and potential spatial separation of gas distribution.** Such discrepancies complicate efforts to precisely investigate or leverage the synergistic effects of NO and CO under pathophysiological conditions. Moreover, these existing systems **offer no means to track the gas release process**, limiting insight into their spatiotemporal behavior.

The second category comprises organic small-molecule platforms capable of co-releasing NO and CO from a single chemical structure. To date, only two representative small molecules have been reported by other groups, *i.e.* Zobi et al. (*Dalton Trans.* **2016**, *45*, 1504–1513) and Hu et al. (*Angew. Chem. Int. Ed.* **2022**, *61*, e202112782). In contrast to co-formulated donor systems, these integrated platforms ensure **localized release** of both gases, minimizing variability caused by differential uptake and distribution. However, due to differences in NO and CO release pathways, the dual-release systems developed by Zobi and Hu still exhibit **disparate release kinetics**, which may limit their therapeutic synergy. To address this challenge and achieve truly **concurrent, co-localized release**, in this work we developed a **cascade-type donor, AhCR565**, which integrates both NO and CO release within a unified photochemical pathway. Furthermore, this platform features a strong rhodamine-based fluorescence turn-on accompanying gas release, enabling **real-time tracking** of dual-gas release without the need for external NO or CO probes. This provides a **robust self-reporting mechanism** for monitoring gas delivery in complex biological systems, offering advantages in imaging clarity, operational simplicity, and translational potential. Moreover, **AhCR575** can be synthesized through a simple and efficient procedure. A comparative summary of the key photochemical properties—including molecular structure, dual gas release mode, release efficiency, tracking capability, and biological application—between our donor and the dual NO/CO-releasing systems reported by Zobi and Hu is provided in **Table S2** for clarity.

Table S2. Comparison of our work with two previously reported molecular NO and CO dual-release systems by other groups.

	Zobi et al.	**Hu et al.**	**This work (AhCR565)**
Ref	*Dalton Trans.* **2016**, *45*, 1504–1513.	*Angew. Chem. Int. Ed.* **2022**, *61*, e202112782.	
Structural characteristic	*N*-Nitrosamine-{cis-$Re[CO]_2\}^{2+}$ cobalamin conjugate	*N*-nitrosamine + 3-HF (incorporated it into block copolymers)	An acylhydrazine-caged rhodamine with N-nitrosamine (small molecule)
Molecular structure	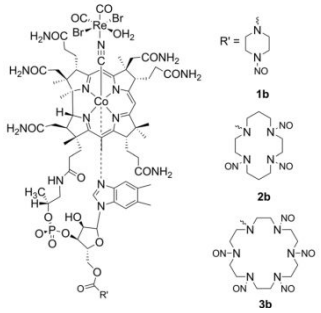	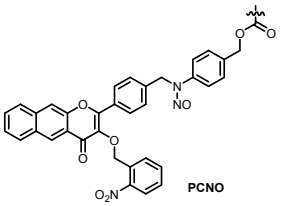	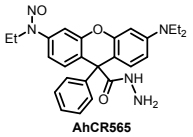
Molecular weight (Da)	>3000 (metal-complex + B12)	678 (monomer) > 8 kDa (diblock copolymer)	459 (drug-like small molecule)
Synthetic complexity	High (organometallic synthesis + B12 conjugation)	Moderate to high (multi-step polymer synthesis)	Low (three-step modular synthesis)
Gas release trigger	Spontaneous in buffer (no external control)	Light (410 nm)	Light (365 - 560 nm)
Controllability of release	No (passive, uncontrollable)	Partial (independent photo-release)	Yes (cascade release with single-wavelength control)
Mechanism of gas release	Decomposition	Independent NO and CO release pathways	Photo-cascade: NO release triggers CO release
Quantum yield (Φ)	Not reported	29.6% (410 nm)	0.087% (520 nm); 3.664% (400 nm)
NO release efficiency	**1b**: 3.9%; **2b**: 3.6%; **3b**: 8.7%	45%	76.2%
CO release efficiency	Not reported	16 ppm in tested condition	30.5%
Fluorescence reporting	No signal change	Turn-off signal (603 nm)	Turn-on signal (565 nm)
Real-time tracking	No	Partial (potentially affected by photobleaching)	Yes (fluorogenic and robust)
Biological validation	Cytoprotection in 3T3 cells (no synergy vs. NORM/CORM)	Antibacterial synergy *in vitro* and in MRSA-infected wounds	Antibacterial synergy *in vitro* and in MRSA-infected wounds (bacterial clearance, wound healing)

Additional Discussion

The antibacterial efficacy of NO and CO is highly dependent on their release form, localization, and kinetics, and that the optimal therapeutic doses can vary significantly across different delivery systems and bacterial models (*ACS Biomater. Sci. Eng.* **2020**, *6*, 433-441; *ChemMedChem* **2021**, *16*, 1–8; *Bioac. Mater.* **2023***, 23, 129–155*). **For NO**, literature reports suggest that concentrations in the submicromolar to micromolar range can exert potent antibacterial activity. Howlin et al. demonstrated that submicromolar levels of nitric oxide (NO) were effective in combating *Pseudomonas aeruginosa* infections in cystic fibrosis, significantly enhancing the susceptibility of *P. aeruginosa* biofilms to tobramycin, both alone and in combination with ceftazidime (*Mol. Ther.* **2017**, *25(9)*, 2104–2116.). Another study by Hu et al. showed that a NO donor releasing around 70 μM NO achieved marked bacterial killing against *Pseudomonas aeruginosa in vitro* (*Angew. Chem. Int. Ed.* **2021**, *60*, 20452-20460). **For CO**, relatively higher concentrations, typically in the hundreds of micromolar range, are generally required to achieve comparable antibacterial effects. For instance, Saraiva et al. reported that organometallic complexes, including tricarbonyldichlororuthenium(II) dimer (CORM-2), tricarbonylchloro(glycinato)ruthenium(II) (CORM-3), bromo(pentacarbonyl)manganese (ALF021), and tetraethylammonium molybdenum pentacarbonyl bromide (ALF062), required 100–500 μM CO equivalents to exhibit potent antibacterial activity toward *E. coli* and *S. aureus in vitro* (*Antimicrob. Agents Chemother.* **2007**, *51*(12), 4303–4307). However, DesMard et al. demonstrated that CORM-3 exhibited dose-dependent antibacterial activity, with concentrations ranging from 0.5 to 10 μM leading to varying degrees of *P. aeruginosa* growth inhibition (*ASEB J.* **2009**, *23* (4), 1023–1031). No definitive optimal concentration has been established so far, as reported efficacies vary across studies.

Given that NO and CO exhibit distinct yet complementary mechanisms in infected wound therapy—the concept of dual gas therapy has attracted increasing attention. Over the past decade, several delivery platforms have been developed for the simultaneous or localized release of both gases in bacterial infections and other diseases contexts. These include organic small molecules, copolymers, hydrogel patches, and upconversion nanoparticles (see Table S3 for comparison). Notably, ***systems enabling a roughly equimolar release of NO and CO have demonstrated synergistic antibacterial effects*** (*Angew. Chem. Int. Ed.* **2022**, *61*, e202112782; *Chem. Eng. J.* **2024**, *480*, 147850), even though these release ratios may not exactly align with the individually optimized concentrations determined from single-gas studies.

Accordingly, while we acknowledge that equimolar release may not represent the ideal therapeutic dosing profiles of NO and CO in all infection models, previous studies—as well as our own data—suggested that ***such comparable ratios can still achieve biologically meaningful synergy***. This supports the feasibility and practical value of comparable dual gas therapy platforms as a rational starting point, with room for further optimization in future therapeutic design. Given the current variability across experimental models, gas donor systems, and pathological conditions—and considering the limited number of dual gas delivery systems reported to date—***the optimal dosing concentrations and NO:CO molar ratios remain to be systematically investigated and fully elucidated***. Further in-depth investigations will be critical to unlocking the full therapeutic potential of this approach and guiding rational dose design for specific clinical scenarios.

Table S3. Representative NO and CO co-delivery systems with dosage information and biological evaluations.

Delivery System Type	Trigger Mechanism		System Dosage	NO donor Dose	CO donor Dose	NO:CO Molar Ratio	Biological validation
Zobi et al. *Dalton Trans.* **2016**, *45*, 1504–1513.							
Organic small molecule	Spontaneous in buffer (no external control)	*in vitro*	30 μM	30 μM	30 μM	1:2 to 5:2	Cytoprotection in ischemia-reperfusion 3T3 cells (no synergy vs. NORM/CORM)
		in vivo	/	/	/	/	/
Hu et al. *Angew. Chem. Int. Ed.* **2022**, *61*, e202112782.							
Block copolymers	Light (410 nm)	*in vitro*	100 μg/mL	/	/	1:1	Antibacterial synergy against MRSA
		in vivo	100 μg/mL (15 μL)	/	/	1:1	Antibacterial synergy in MRSA-infected wounds
Yang et al. *Nat. Commun.* **2023**, *14*, 2417.							
hydrogel patch	Spontaneous hydrolysis	*in vitro*	/	400 μM	200 μM	2:3	HUVECs cell migration
		in vivo	/	400 μM (500 μL per choke zone)	200 μM (500 μL per choke zone)	2:3	Synergistic Ischemia-reperfusion dorsal skin flap model in rats
Xu et. *ACS Appl. Mater. Interfaces* **2023,** *15*, 56796–56806.							
Upconversion nanoparticles	808 nm light irradiation	*in vitro*	20 μg/mL	3.4 μg/mL	1.7 μg/mL	~1:1	Induced synergistic apoptosis in HCT116 and CT26 colon cancer cells
		in vivo	/	10 mg/Kg	5 mg/Kg	~1:1	Synergistically inhibits colon tumor growth
Zhang et al. *ACS Appl. Bio Mater.* **2024**, *7*, 7585–7594							
Upconversion nanoparticles	Ultrasound	*in vitro*	/	2.28 μg/mL	2.28 μg/mL	~1:2	Trigger CT26 cells apoptosis synergistically
		in vivo	/	7.5 mg/Kg	7.5 mg/Kg	~1:2	Synergistic cancer gasotherapy
Wang et al. *Chem. Eng. J.* **2024**, *480*, 147850							
Upconversion nanoparticles	808 nm light irradiation	*in vitro*	250 μg/mL	13.75 μg/mL	16.25 μg/mL	2:7	Antibacterial and antiinflammation
		in vivo	1 mg/mL (200 μL)	0.055 mg/mL (200 μL)	0.065 mg/mL (200 μL)	2:7	Synergistic therapy against periodontitis
Hu et al. *Angew. Chem. Int. Ed.* **2025**, *64*, e202419939							
Micelle	630 nm light irradiation	*in vitro*	50 μg/mL	16.7 μg/mL	33.3 μg/mL	~1:2	Synergistically impaired mitochondrial function
		in vivo	30 mg/kg	10 mg/kg	20 mg/kg	~1:2	Synergistically inhibit 4T1 tumor

Our group. *J. Am. Chem. Soc.* **2024**, *146(44)*, 30361−30371.							
Organic small molecule	520 nm light irradiation	*in vitro*	2 μM	2 μM	2 μM	1:1	/
		in vivo	2 mM (6 μL)	2 mM (6 μL)	2 mM (6 μL)	1:1	Synergistic glaucoma therapy
This work.							
Organic small molecule	520 nm light irradiation	*in vitro*	1-4 μM	1-4 μM	1-4 μM	1:1	Antibacterial synergy against MRSA
		in vivo	5 mg/kg (10 μL)	5 mg/kg (10 μL)	5 mg/kg (10 μL)	1:1	Antibacterial synergy in MRSA-infected wounds

Note: "/" indicates *not reported* or *not applicable*. The NO:CO molar ratios listed in the table are theoretical values based on the design of the co-delivery systems. In cases where the exact encapsulation efficiency or actual gas release amounts were not reported, the ratios were estimated based on the initial loading amounts of NO and CO donors, as well as reported formulation parameters such as donor feeding ratios and encapsulation efficiencies.

Reference

1. Yin L.; Zhao B.; Zhou J.; Huang Y.; Ma H.; Zhou T.; Mou J.; Min P.; Chen J.; Ge G.; Qian X.; Luo X.; Yang Y. A Carbon‐Caged Rhodamine Generating Nitrosoperoxycarbonate for Photoimmunotherapy. *Angew. Chem. Int. Ed.* **2024**, *63*, e202402949.
2. Li J.; Dong Y.; Wei R.; Jiang G.; Yao C.; Lv M.; Wu Y.; Gardner S. H.; Zhang F.; Lucero M. Y.; Huang J.; Chen H.; Ge G.; Chan J.; Chen J.; Sun H.; Luo X.; Qian X.; Yang Y. Stable, Bright, and Long-Fluorescence-Lifetime Dyes for Deep-Near-Infrared Bioimaging. *J. Am. Chem. Soc.* **2022**, *144*, 14351-14362.
3. Snellenburg, J.; Laptenok, S.; Seger, R.; Mullen, K.; Stokkum, I. V. Glotaran: A Java-Based Graphical User Interface for the R Package TIMP. *J. Stat. Softw. Statal.* **2012**, *49*, 1-22.
4. Feng, S.; Liu, D.; Feng, W.; Feng, G. Allyl Fluorescein Ethers as Promising Fluorescent Probes for Carbon Monoxide Imaging in Living Cells. *Anal. Chem.* **2017,** *89*, 3754-3760.
5. Luo, X.; Yang, H.; Wang, H.; Ye, Z.; Zhou, Z.; Gu, L.; Chen, J.; Xiao, Y.; Liang, X.; Qian, X.; Yang, Y. Highly Sensitive Hill-Type Small-Molecule pH Probe That Recognizes the Reversed pH Gradient of Cancer Cells. *Anal. Chem.* **2018,** *90*, 5803-5809.
6. Luo, X.; Zhang, Z.; Wang, J.; Wang, X.; Zhang, Y.; Chen, J.; Ge, G.; Yang, W.; Qian, X.; Tian, Y.; Yang, Y., Acyl-caged rhodamines: photo-controlled and self-calibrated generation of acetyl radicals for neural function recovery in early AD mice. *Chem. Sci.* **2023,** *14*, 11689-11698.